Generic planar phase resetting near a phaseless point

Kyoung Hyun Lee* Neil G. R. Broderick†
Bernd Krauskopf* Hinke M. Osinga*

October 2024

Abstract

We study the planar FitzHugh-Nagumo system with an attracting periodic orbit that surrounds a repelling focus equilibrium. When the associated oscillation of the system is perturbed, in a given direction and with a given amplitude, there will generally be a change in phase of the perturbed oscillation with respect to the unperturbed one. This is recorded by the phase transition curve (PTC), which relates the old phase (along the periodic orbit) to the new phase (after perturbation). We take a geometric point of view and consider the phase-resetting surface comprising all PTCs as a function of the perturbation amplitude. This surface has a singularity when the perturbation maps a point on the periodic orbit exactly onto the repelling focus, which is the only point that does not return to stable oscillation. We also consider the PTC as a function of the direction of the perturbation and present how the corresponding phase-resetting surface changes with increasing perturbation amplitude. In this way, we provide a complete geometric interpretation of how the PTC changes for any perturbation direction. Unlike what has been reported in the literature so far, the FitzHugh–Nagumo system is a generic example and, hence, representative for other planar vector fields.

2020 MSC codes: 34C15, 37C27, 65L10, 92B25
keywords: Phase transition curve, isochrons, phase transition surface, phase singularity.

*Department of Mathematics and Dodd–Walls Centre for Photonic and Quantum Technologies, University of Auckland, Private Bag 92019, Auckland 1142, New Zealand.
†Department of Physics and Dodd–Walls Centre for Photonic and Quantum Technologies, University of Auckland, Private Bag 92019, Auckland 1142, New Zealand.

1 Introduction

Phase resetting is a technique that is often applied in neuroscience to study the behaviour and properties of neuronal firing patterns [3, 18]. In essence, given a stable cyclic oscillation, denoted Γ, a phase reset is the act of applying a perturbation of a particular strength, in a particular direction, and recording the resulting phase shift upon return to Γ with respect to the phase at which the perturbation was applied. Phase resetting is strongly related to the notion of isochrons, which each comprise all points that converge to Γ with a given phase: the phase reset maps a point on Γ to a perturbed point that lies on a particular isochron and, hence, returns to Γ with the phase associated with this isochron. Winfree [21] devoted most of his career to the study of isochrons and the properties of so-called phase transition and phase response curves, which relate the 'old' phase ϑ_{o} along Γ with the 'new' phase ϑ_{n} and phase shift $\vartheta_{\mathrm{n}} - \vartheta_{\mathrm{o}}$, respectively, that result from a given fixed perturbation. Winfree defined the old and new phases as fractions of the total time needed to complete one oscillation; hence, $\vartheta_{\mathrm{o}}, \vartheta_{\mathrm{n}} \in [0, 1)$ are defined on the circle $\mathbb{S}^1 := \mathbb{R}/\mathbb{Z}$.

Winfree's classical paper on isochrons [20] defines a *latent* phase for each point in the basin of attraction of Γ for a given system of first-order differential equations (a vector field). Winfree made a series of conjectures regarding the properties of isochrons that were later confirmed by Guckenheimer [7] who realised that isochrons are, in fact, stable manifolds of fixed points given by the fixed-time return map associated with the period T_Γ of Γ. Normally hyperbolic invariant manifold theory [10], which at the time was still being developed, implies that the family of isochrons, parametrised by the phase $\vartheta_{\mathrm{o}} \in [0, 1)$, foliates the basin of attraction of Γ; this means that any point in the basin lies on exactly one isochron (of a specific phase) in the family. Since isochrons are global invariant manifolds, they are not known analytically (except in very special cases) and need to be computed with advanced numerical tools [12, 16].

In this paper, we study phase resets for the FitzHugh–Nagumo system [5, 15], which is a planar, polynomial system that will be introduced in the next section; see already system (1). The parameters for the FitzHugh–Nagumo system are chosen such that it has an attracting periodic orbit Γ, and our interest lies in the possible behaviour of its phase transition curves (PTCs) that relate the new phase ϑ_{n} to the old phase ϑ_{o} before the reset. Note that, certainly for planar systems, not all points in the phase space converge to Γ, and phase resets are meant to involve only resets to points in the basin of attraction of Γ; discontinuities arise when resets occur to points in the so-called phaseless set, which consists of all points outside of the basin of

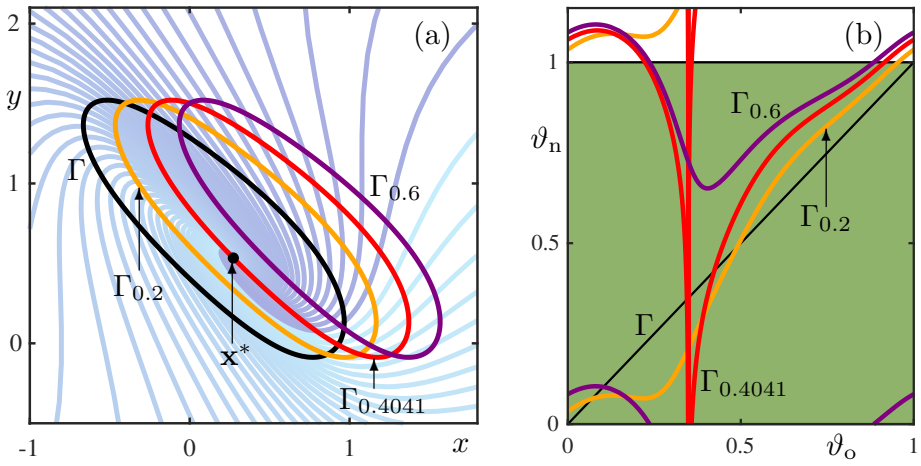

Figure 1: Phase resets for the FitzHugh–Nagumo system (1) in the x-direction for perturbation amplitudes $A = 0.2$, $A = A_c \approx 0.4041$, and $A = 0.6$. Panel (a) shows the periodic orbit Γ (black) overlayed on 50 isochrons uniformly distributed in phase, coloured from phase 0 (cyan) to 1 (dark blue). Also shown are the shifted perturbation sets $\Gamma_{0.2}$ (orange), $\Gamma_{0.4041}$ (red), $\Gamma_{0.6}$ (purple), with the resulting PTCs shown in matching colours in panel (b) over an extended ϑ_n-range, where the fundamental square in the $(\vartheta_\mathrm{o}, \vartheta_\mathrm{n})$-plane is highlighted (green shading).

attraction. For the FitzHugh–Nagumo system, we encounter a phaseless set that is quite typical for planar vector fields [12, 14, 16]: it comprises a single point, denoted $\boldsymbol{x}^*$, which is a repelling focus equilibrium.

Figure 1 illustrates three phase resets for the FitzHugh–Nagumo system. Panel (a) shows Γ together with 50 isochrons I_ϑ that are uniformly distributed in phase; the isochrons are shaded in increasingly darker colours for increasing $\vartheta \in [0, 1)$. All isochrons are transverse to Γ and accumulate on $\boldsymbol{x}^*$ sufficiently slowly in a clockwise spiralling fashion. A perturbation is applied to each point along Γ, in the horizontal direction (parallel to the x-axis). Hence, Γ is effectively shifted horizontally by the perturbation amplitude A, chosen as $A = 0.2$, $A = A_c \approx 0.4041$ and $A = 0.6$, which gives the shifted perturbation sets labelled $\Gamma_{0.2}$, $\Gamma_{0.4041}$ and $\Gamma_{0.6}$, respectively. The resulting three PTCs are shown in panel (b) over an extended range of ϑ_n; here and in subsequent figures, the region with $(\vartheta_\mathrm{o}, \vartheta_\mathrm{n}) \in [0, 1) \times [0, 1)$ is highlighted, because it is the 'fundamental square' in the $(\vartheta_\mathrm{o}, \vartheta_\mathrm{n})$-plane representing the torus $\mathbb{S}^1 \times \mathbb{S}^1$ (by identifying the left and right, and top an bottom sides). The local maxima and minima of the PTCs arise when the perturbation set is tangent to one of the isochrons in the family; in Fig. 1(a), such tangencies occur, for

example, near the minimum of the shifted perturbation sets (leading to a local maximum of the PTCs).

Note that the perturbation set $\Gamma_{0.4041}$ in Fig. 1(a) passes exactly through the repelling focus $\boldsymbol{x}^*$ around which the isochrons spiral; indeed, $A = A_c$ is the unique perturbation amplitude with this property, and we refer to it as the critical amplitude A_c. Its relevance is the following. For the perturbation amplitude $A = 0.2$ well before A_c, the perturbation set Γ_A crosses all isochrons, meaning that the PTC covers the full range of $\vartheta_\mathrm{n} \in [0, 1)$. Figure 1(b) shows that the PTC for $A = 0.2$ can be viewed as a smooth deformation of the diagonal, which corresponds to a phase reset with $A = 0$, that is, to Γ itself. Note that the PTC for $A = 0.2$ is a continuous smooth curve on the torus $\mathbb{S}^1 \times \mathbb{S}^1$, represented by the fundamental square $[0, 1] \times [0, 1]$. Similarly, when $A = 0.6$ past A_c, the perturbation set Γ_A crosses only a subset of the isochron family. The resulting PTC in Fig. 1(b) is again a smooth curve on the torus, but it is now topologically different. Indeed, for $0 \leq A < A_c$, the PTC is a $1:1$ torus knot, while for $A > A_c$ it is a $1:0$ torus knot [13, 17].

Precisely at $A = A_c$, the PTC is singular: the point on Γ with phase $\vartheta_\mathrm{o} \approx 0.3484$ resets to $\boldsymbol{x}^*$. In Fig. 1(b), ϑ_n approaches negative infinity in the covering space $\mathbb{R}$ of ϑ_n as this value of ϑ_o is approached from either side. Winfree referred to such an event as *oscillator death* [22], and he realised that it separates the above topologically different cases of PTCs; see also [1, 6]. Remarkably, Winfree was able to construct an idealised sketch of a surface in $(\vartheta_\mathrm{o}, A, \vartheta_\mathrm{n})$-space [19, Fig. 5], based on about 300 experimental data points resulting from phase reset experiments (on yeast cells) at varying phases ϑ_o and perturbation amplitudes A. He observed that his sketch resembles a 'spiral staircase rising counterclockwise' and explained that the rotation axis points to an isolated singular stimulus in the $(\vartheta_\mathrm{o}, A)$-plane; the singular stimulus is precisely the perturbation with amplitude $A = A_c$ that leads to an interaction with $\boldsymbol{x}^*$. More precisely, Winfree's surface is a helix with its axis the vertical line through the point $(\vartheta_\mathrm{o}, A)$ with $A = A_c$ and ϑ_o the phase of the point on Γ that resets to $\boldsymbol{x}^*$ for this critical perturbation amplitude. However, Winfree's spiralling staircase is not the typical situation for resets interacting with a single phaseless point. Mathematically speaking, his helical surface only appears if the isochrons are *not spiralling* around the phaseless point. We suspect that the expansion rate near the phaseless point (relative to the difference in rotation speed) was so strong that the spiralling behaviour could not be resolved in his experiment.

In this paper, we present the FitzHugh–Nagumo system as the typical case of phase resetting in a planar system with a phaseless point. Specifically, the requirement is that the isochrons spiral around this point because there is (generically) a difference between the period of Γ and the rotational

speed around the phaseless point. We made this point in previous work [14], where we studied a family of planar model vector fields, also due to Winfree, for which the isochrons are known explicitly. However, that example has rotational symmetry and, hence, is highly non-generic. More generally, studies to date of changes in the PTC for varying perturbation amplitudes focused on similar simplified examples [3, 12, 14, 20] that exhibit symmetries to aid in the analysis, or on very realistic models [1, 6, 13, 16, 17, 18] with a complexity that obscures the essential underlying mechanisms. In contrast, the FitzHugh–Nagumo system has no symmetries and the difference in rotation speeds around Γ and $\boldsymbol{x}^*$ is sufficiently large to observe the details of the generic changes of the PTC, as the perturbation amplitude A is increased through A_c. This is in contrast to the example of the Van der Pol system that was also studied in [14], but for which the difference in rotation speed turned out to be too small — much like what we suspect was the case in Winfree's experiment [19]. Moreover, the Van der Pol system still has a symmetry; namely, it is invariant under rotation by π around the origin, which is the phaseless point.

In this paper, we show that, as A increases through A_c, there is an infinite sequence of *twin tangencies*, where the phase reset is such that the shifted periodic orbit Γ has two separate points of tangency with one and the same isochron. Each such twin tangency changes how many times the unit interval of ϑ_n is covered by the PTC, which increases to infinity as $A \nearrow A_c$ and then decreases again past $A = A_c$. We are able to identify and illustrate clearly such twin tangencies of the FitzHugh–Nagumo system — which is a first for a generic planar vector field. Moreover, we discuss how these changes of the PTC (for a given direction of perturbation) are encoded by the geometry of the phase-resetting surface in $(\vartheta_\mathrm{o}, A, \vartheta_\mathrm{n})$-space. Colloquially speaking, owing to the spiralling nature of the isochrons near ϑ_n, this surface rolls up around a singular vertical line at $A = A_c$ and the corresponding value of ϑ_o, and this has the observed consequences for the transition of the PTC. We also present a discussion of phase resets with perturbations in different directions (given by an angle φ_d), which are associated with different values of A_c and ϑ_o. To this end, we present the phase-resetting surface in $(\vartheta_\mathrm{o}, \varphi_\mathrm{d}, \vartheta_\mathrm{n})$-space, and show how it changes with the perturbation amplitude A. To obtain these results we compute isochrons and PTCs with a boundary-value problem setup that was implemented within the package CoCo [2]; see [9, 13, 16] for more details.

This paper is organised as follows. In Sec. 2 we introduce the FitzHugh–Nagumo system and state the specific parameter values we use. Section 3 then introduces its PTC for a perturbation in the positive x-direction, and how the PTC is defined as the graph of a function $\mathcal{P}_A$ that depends on the

Winfree's values	no time-scale separation	off-set from origin
$a = 0.7$ $b = 0.8$	$c = 1$	$z = -0.8$

Table 1: The values of the parameters of the FitzHugh–Nagumo system (1) that are used throughout.

perturbation amplitude A. This includes a discussion of the loss of invertibility of the map $\mathcal{P}_A$ in Sec. 3.1, and its changes due to twin tangencies in Sec. 3.2; the associated phase-resetting surface in $(\vartheta_\mathrm{o}, A, \vartheta_\mathrm{n})$-space is introduced and presented in Sec. 3.3. In Sec. 4, we discuss the influence of the direction of the perturbation, as represented by the angle φ_d; the five qualitatively different cases of the phase-resetting surface for fixed A are presented and discussed in Sec. 4.1. We present in Sec. 5 a discussion and brief outlook on possible future work.

2 The FitzHugh–Nagumo system

Winfree [21] studied the FitzHugh–Nagumo system [5, 15] as a typical planar example that cannot be analysed explicitly. He wrote the system as

$$\left\{ \begin{array}{rcl} \dot{x} &=& c\,(y + x - \frac{1}{3}\,x^3 + z), \\ \dot{y} &=& -\frac{1}{c}\,(x - a + b\,y), \end{array} \right. \tag{1}$$

and his interest was in the regime for which this system has an attracting periodic orbit with a repelling focus equilibrium as the single phaseless point. His numerical explorations suggested that the isochron structure is extremely complicated, which was later confirmed with more advanced computational methods [11]. An immediate consequence of such a complex isochron structure is that the FitzHugh–Nagumo system may feature complicated PTCs for phase resets well before the interaction with the phaseless point [13]. One particular reason for this complexity is a significant difference in time scales between the evolutions of the x- and y-coordinates, as given by the choice for the parameter c [12].

We consider system (1) in the same parameter regime as Winfree, but set $c = 1$, so that there is effectively no time-scale separation; moreover, we introduce the off-set $z = -0.8$ to move the equilibrium away from the origin. This choice of parameter values is given in Table 1, and it results in the overall structure of isochrons of the FitzHugh–Nagumo system as illustrated in Fig. 1(a). More specifically, system (1) has the attracting periodic orbit Γ of period $T_\Gamma \approx 10.8329$, with the zero-phase point $\gamma_0 \approx (0.9660, 0.1345) \in \Gamma$,

defined (by convention in the field) as the point with the maximum value of the x-coordinate. The motion along Γ is clockwise, and it surrounds the repelling focus $\boldsymbol{x}^* \approx (0.2729, 0.5339)$ with eigenvalues $0.0628 \pm 0.5056\, i$, which constitutes the phaseless set. Since the rotation period around $\boldsymbol{x}^*$ is larger than T_Γ, the isochrons of Γ spiral around $\boldsymbol{x}^*$ in the clockwise direction; see Fig. 1(a).

3 PTCs for varying perturbation amplitude

The three PTCs illustrated in Fig. 1 for the FitzHugh–Nagumo system (1) with parameters as in Table 1 are only part of the story of the transition from a $1:1$ to a $1:0$ torus knot. As the perturbation amplitude A increases towards A_c, the PTC changes dramatically. To aid the discussion, we define the *phase-resetting function*

$$\mathcal{P}_A : \vartheta_\mathrm{o} \in [0,1) \to \vartheta_\mathrm{n} \in [0,1) \tag{2}$$

as the function from the old to the new phase, which has the PTC with given perturbation amplitude $A \geq 0$ as its graph $\mathrm{graph}(\mathcal{P}_A)$. Throughout this section, we consider exclusively perturbations in the fixed direction of increasing x, as was done in Fig. 1; this is natural in terms of the neurophysiological interpretation of the FitzHugh–Nagumo system because resets are typically achieved by voltage input [5, 15]. The phase-resetting function $\mathcal{P}_0$ (in the absence of a perturbation) is the identity, meaning that the PTC for $A = 0$ is the diagonal, labelled Γ in Fig. 1(b) and similar figures. In particular, this means that $\mathcal{P}_A$ is invertible when A is sufficiently small. However, when A becomes too large, invertibility of $\mathcal{P}_A$ is lost.

3.1 Loss of invertibility

Figure 2 illustrates the loss of invertibility in the style of Fig. 1 with the perturbation sets and PTCs for $A = 0.08$, $A = 0.1793$, and $A = 0.28$. Panels (a1) and (a2) of Fig. 2 show Γ with the three shifted perturbation sets together with three highlighted isochrons, and panels (b1) and (b2) show the corresponding PTCs. The perturbation set Γ_A for $A = 0.08$ intersects all isochrons transversely and, consequently, $\mathcal{P}_A$ is invertible and the PTC is monotonically increasing. At $A \approx 0.1793$ the perturbation set has a cubic tangency with the isochron $I_{0.0820}$, which means that the PTC has an inflection point at the value $\vartheta_\mathrm{n} = 0.0820$; see the enlargement panels (a2) and (b2). For larger values of A the perturbation set Γ_A has quadratic tangencies with two different isochrons; for the case $A = 0.28$ shown in Fig. 2, these are

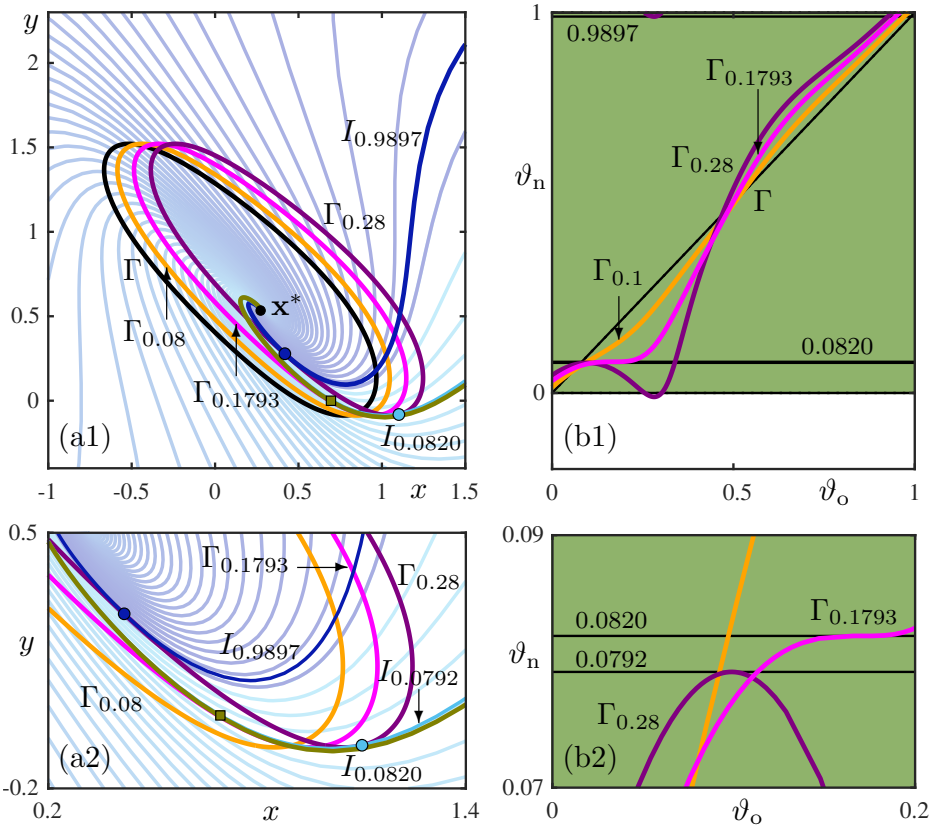

Figure 2: Transition through the cubic tangency at $A \approx 0.1793$. Panel (a1) shows Γ (black), $\Gamma_{0.08}$ (orange), $\Gamma_{0.1793}$ (magenta), and $\Gamma_{0.28}$ (purple), along with the isochrons $I_{0.0792}$ (cyan), $I_{0.0820}$ (olive), and $I_{0.9807}$ (dark blue), and panel (b1) shows the corresponding PTCs in matching colors. Panels (a2) and (b2) are respective enlargements near the cubic tangency.

$I_{0.0792}$ and $I_{0.9897}$. As a consequence, the PTC is no longer invertible: for $A = 0.28$ it has a local maximum and a local minimum, with $\vartheta_n = 0.0792$ and $\vartheta_n = 0.9897$, respectively, for $A = 0.28$. Indeed, Figure 2 clearly illustrates that the loss of invertibility of the PTC is due to the cubic tangency of the perturbation set with an isochron; see also [13, 17].

3.2 First and last twin tangency

As A is increased further towards A_c, the local maximum of the PTC moves up in ϑ_n and its local minimum moves down. When viewed in the covering space, as in Fig. 2(b1), the two extrema move further and further apart, and their difference in ϑ_n becomes an integer for special values of A. When

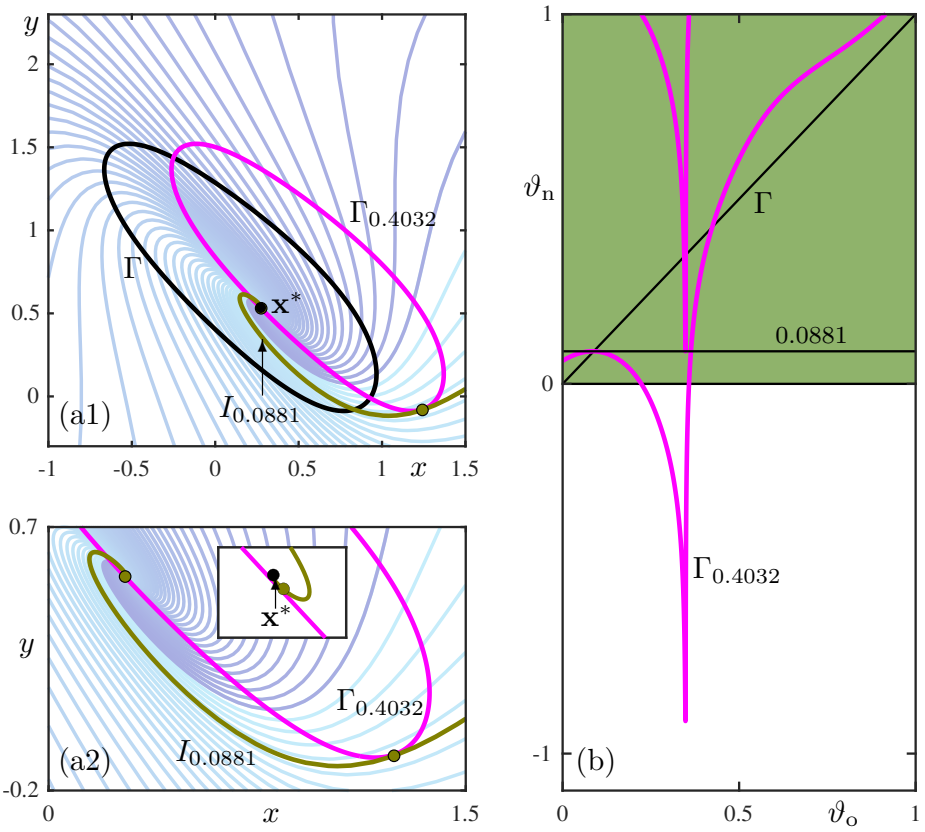

Figure 3: The first twin tangency at $A \approx 0.4032 < A_c$. Panel (a1) shows Γ (black) with $\Gamma_{0.4032}$ (magenta) and the isochron $I_{0.0881}$ (olive), and panel (a2) with its inset show successive enlargements near the twin tangency points. The corresponding PTC is shown in panel (b) over an extended range of ϑ_n.

ϑ_n is taken modulo 1 on the fundamental square, the local maximum and minimum then have equal values, which marks a transition in terms of how many times the full range of $\vartheta_\mathrm{n} \in [0, 1)$ is covered by $\mathcal{P}_A$ and, hence, the PTC. Geometrically, this means that there are two (quadratic) tangencies between the perturbation set and one and the same isochron, given by the ϑ_n-value of the simultaneous maximum and minimum. We call this a *twin tangency* and Fig. 3 illustrates the first one as A is increased, which occurs approximately at $A \approx 0.4032$. Panel (a1) shows that $\Gamma_{0.4032}$ is tangent to the single isochron $I_{0.0881}$ at two different points; note from the enlargements in panel (a2) that one of these tangencies is very close to the phaseless point $\boldsymbol{x}^*$. The representation of the PTC over an extended ϑ_n-range illustrates that its maximum and minimum have a difference of 1 in the covering space and, hence, have the same ϑ_n-value in the fundamental square. Notice that

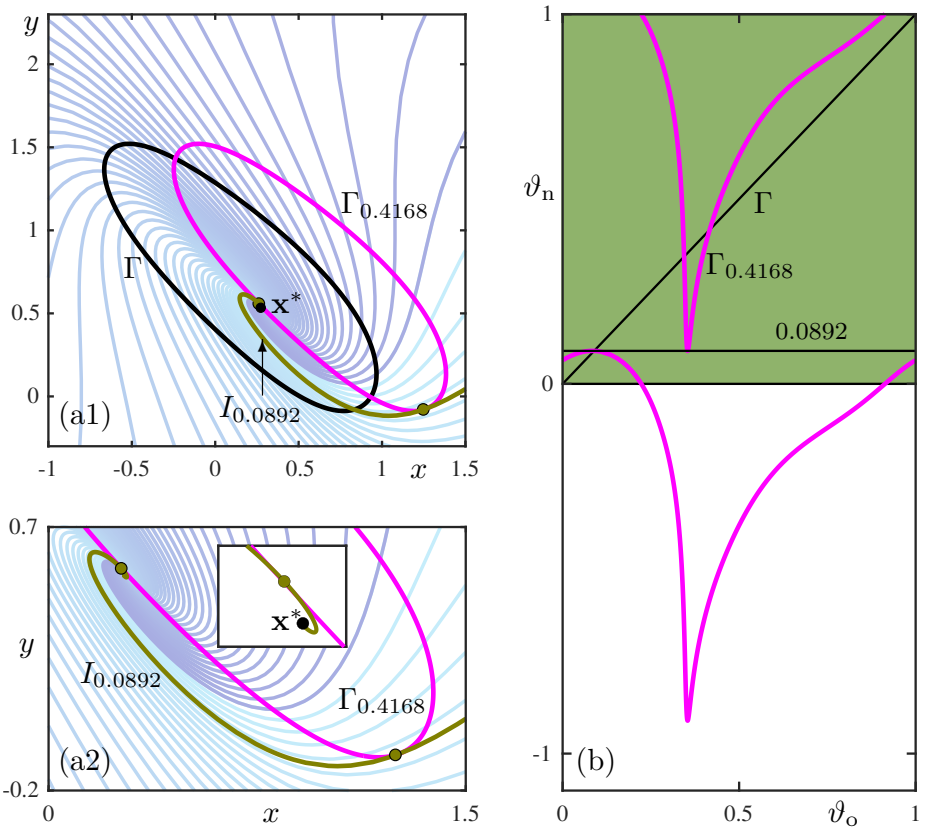

Figure 4: The last twin tangency at $A \approx 0.4168 > A_c$. Panel (a1) shows Γ (black) with $\Gamma_{0.4168}$ (cyan) and the isochron $I_{0.0892}$ (olive), and panel (a2) and its inset are successive enlargements near the twin tangency points. The corresponding PTC is shown in panel (b) over an extended range of ϑ_n.

$\Gamma_{0.4032}$ intersects every isochron precisely three times; equivalently, the PTC in Fig. 3(b) covers the ϑ_n-range $[0, 1)$ of the torus precisely three times; note that the PTC remains a $1:1$ torus knot (ϑ_n still increases by 1 with $\vartheta_\mathrm{o} \in [0, 1)$). As A increases further towards A_c, the minimum of the PTC moves towards lower and lower values of ϑ_n in the covering space, such that there is an infinite sequence of twin tangencies, each increasing the number of coverings of the unit interval by 2.

At $A = A_c$, the PTC changes topological type from $1:1$ to a $1:0$ torus knot. This happens in the limit of an infinite covering of the ϑ_n-range $[0, 1)$. For A past the critical value A_c, there is a sequence of twin tangencies in reverse that reduces the number of times the ϑ_n-range $[0, 1)$ is covered; the difference is that, at each twin tangency, the perturbation set Γ_A now crosses all isochrons exactly an even number of times. Figure 4 illustrates

the last twin tangency of this reverse sequence in the style of Fig. 3. As panels (a1) and (a2) of Fig. 4 show, the perturbation set $\Gamma_{0.4168}$ has two points of quadratic tangency with one and the same isochron $I_{0.0892}$. Note that, compared to the first twin tangency, the perturbation set and the second tangency point is now 'on the other side' of the phaseless point $\boldsymbol{x}^*$. The PTC in Fig. 4(b) is now a $1:0$ torus knot that covers $[0,1)$ exactly twice. After the last twin tangency, for $A > 0.4168$, the PTC loses surjectivity and no longer covers the full range of ϑ_n: the transition through A_c is complete; see the case for $A = 0.6$ in Fig. 1(b).

3.3 Phase-resetting surface near its singularity

The entire transition of the PTC through A_c can be represented geometrically by the *phase-resetting surface* consisting of the PTCs for any A. More formally, we now consider the function $\mathcal{P}(\vartheta_\mathrm{o}, A) = \mathcal{P}_A(\vartheta_\mathrm{o})$ over the $(\vartheta_\mathrm{o}, A)$-plane, and the phase-resetting surface of system (1) in $(\vartheta_\mathrm{o}, A, \vartheta_\mathrm{n})$-space is $\mathrm{graph}(\mathcal{P}) = \{\mathrm{graph}(\mathcal{P}_A) \mid A \in \mathbb{R}^{\geq 0}\}$. This surface is shown in Fig. 5(a). Specifically, we plot the phase-resetting surface over the extended ϑ_n-range $[-1,2]$, so that effectively three copies or sheets are shown. Our focus here is on a neighbourhood of the singular parameter point S given by $A = A_c \approx 0.4041$ and $\vartheta_\mathrm{o} \approx 0.3484$, for which the corresponding point on the periodic orbit Γ maps exactly to $\boldsymbol{x}^*$. In $(\vartheta_\mathrm{o}, A, \vartheta_\mathrm{n})$-space, this parameter point S gives rise to a singular vertical line, and the phase-resetting surface spirals around it.

Figure 5(b) shows a different surface, which is obtained by plotting the family of isochrons in (x, y, ϑ)-space as a function of their ϑ_n-values. Here we focus on a region near the phaseless point $\boldsymbol{x}^*$, which similarly gives rise to a singular vertical line, and also show three copies in the extended ϑ_n-range $[-1,2]$. Observe the striking similarity between the phase-resetting surface near S in Fig. 5(a) and the isochron surface near $\boldsymbol{x}^*$ in panel (b). This is explained by the fact that points $(\vartheta_\mathrm{o}, A)$ near S are mapped smoothly and uniquely to points in the (x, y)-plane near $\boldsymbol{x}^*$ by the 'action' of the perturbation, given by $(\vartheta_\mathrm{o}, A) \mapsto \gamma(\vartheta_\mathrm{o}) + (A, 0)$ with $\gamma(\vartheta_\mathrm{o}) \in \Gamma$. Locally near the singular point S and the phaseless set $\boldsymbol{x}^*$, this mapping is a bijection [14]. Hence, the phase-resetting surface in Fig. 5(a) is the diffeomorphic image of the surface of isochrons in Fig. 5(b) under the local inverse. In particular, the level set of the phase-resetting surface for any fixed value of ϑ_n is a spiral that accumulates on (but never reaches) the respective point on the vertical line S. In fact, the surface in Fig. 5(a) was rendered from a selection of such spirals, each of which was computed as a curve for a fixed value of ϑ_n.

The spiralling nature of the phase-resetting surface around the line S in

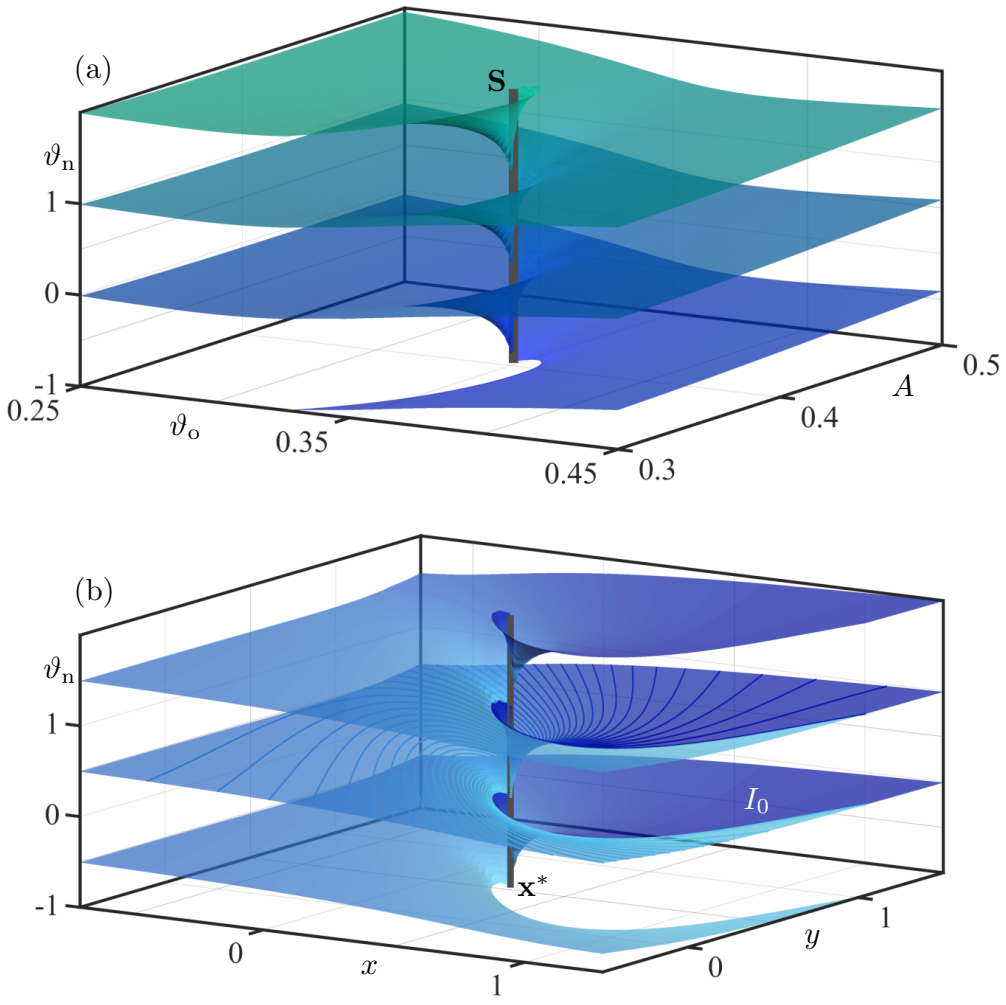

Figure 5: The phase-resetting surface graph($\mathcal{P}_A$) of system (1) in $(\vartheta_o, A, \vartheta_n)$-space near its singular vertical line S in panel (a), and the surface of isochrons in (x, y, ϑ)-space near the phaseless set $\boldsymbol{x}^*$ in panel (b), both shown over the extended ϑ_n-range $[-1, 2]$.

$(\vartheta_o, A, \vartheta_n)$-space is the 'geometric encoding' of the fact that the transition of the PTC, as A is increased through A_c, necessarily involves infinite sequences of twin tangencies, as was discussed in Sec. 3.2. In turn, this is a direct consequence of the spiralling of the isochrons around $\boldsymbol{x}^*$ in the (x, y)-plane. The illustration of this insight in Fig. 5 for the FitzHugh–Nagumo system is for the generic case of a planar vector field; a similar illustration is shown in [14, Fig. 8] for a constructed example due to Winfree with rotational

symmetry and analytically known isochrons.

4 Varying the direction of perturbation

The application context of the FitzHugh–Nagumo system led us to consider only perturbations in the direction of positive x. However, there is actually no mathematical reason for taking the 'traditional' point of view that the direction of the perturbation is fixed. In fact, varying the direction of the perturbation is feasible in experiments, such as those with self-pulsing semiconductor lasers, where a short external input can be applied to the electrical pump current and/or directly to the optical intensity; and coupled oscillators of any sort, where a perturbation may enter at different strengths for different oscillators. This realisation motivates us to extend the earlier definition (2) of the phase resetting function $\mathcal{P}_A$ to include the direction of the perturbation as an additional variable [14]. More precisely, we define the unit direction vector

$$\boldsymbol{d} := \boldsymbol{d}(\varphi_\mathrm{d}) = \begin{bmatrix} \cos(2\pi\,\varphi_\mathrm{d}) \\ \sin(2\pi\,\varphi_\mathrm{d}) \end{bmatrix},$$

for any direction angle $\varphi_\mathrm{d} \in [0,1)$. The definition of $\mathcal{P}_A$ can then be extended to the domain

$$\mathcal{P}_A : \vartheta_\mathrm{o} \in [0,1) \times \varphi_\mathrm{d} \in [0,1) \to \vartheta_\mathrm{n} \in [0,1),$$

where the image ϑ_n is given by the phase of the isochron that contains the point $\gamma(\vartheta_\mathrm{o}) + A\,\boldsymbol{d}(\varphi_\mathrm{d})$, resulting from a reset at the point $\gamma(\vartheta_\mathrm{o}) \in \Gamma$.

For $\varphi_\mathrm{d} = 0$, the unit vector $\boldsymbol{d}(\varphi_\mathrm{d})$ is exclusively in the direction of positive x only, which is the case we considered in Sec. 3. The entire transition scenario of the PTC from $1:1$ to $1:0$ torus knot we presented is generated solely by the fact that perturbation set of the periodic orbit moves through the phaseless point $\boldsymbol{x}^*$ as the perturbation amplitude is increased through the critical amplitude A_c. For $\varphi_\mathrm{d} = 0$, this happens at $A = A_c \approx 0.4041$ and at the unique point $\gamma(\vartheta_\mathrm{o}) \in \Gamma$ of phase $\vartheta_\mathrm{o} \approx 0.3484$. However, since Γ surrounds $\boldsymbol{x}^*$, this will also happen for an increasing perturbation amplitude in any direction, albeit for a different value of the critical amplitude A_c and at a different phase ϑ_o.

Figure 6 illustrates the relationship between A_c, $\vartheta_\mathrm{o} \in [0,1)$ and $\varphi_\mathrm{d} \in [0,1)$. Panel (a) shows Γ together with 50 isochrons evenly distributed in phase. We labelled four points on Γ, which are local extrema of the pointwise distance between Γ and $\boldsymbol{x}^*$. Observe that, for any $\vartheta_\mathrm{o} \in [0,1)$, the point

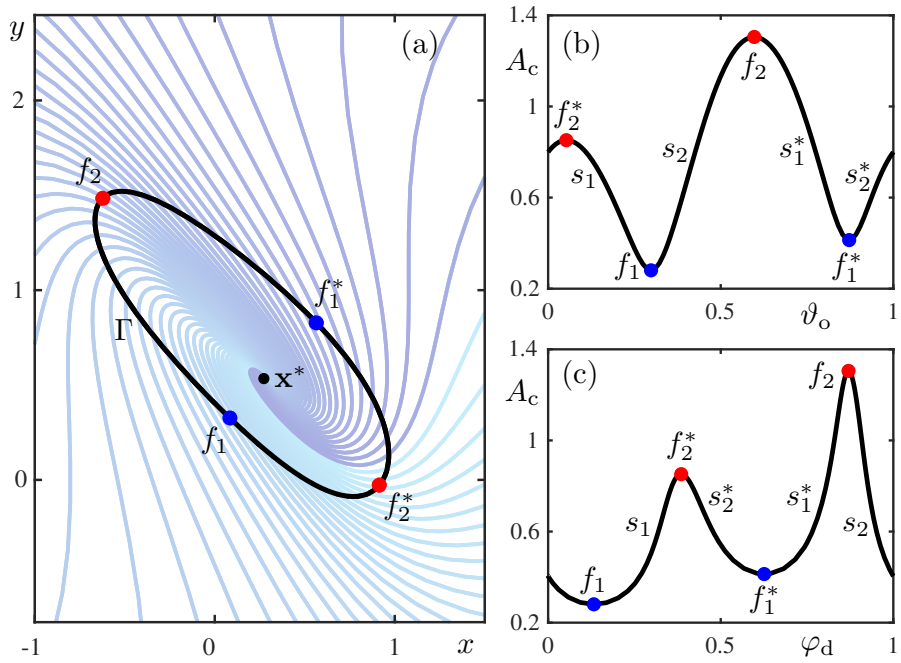

Figure 6: Critical perturbation amplitude A_c in dependence on the perturbation direction $\boldsymbol{d}(\varphi_d)$, with $\varphi_d \in [0,1)$, and phase $\vartheta_o \in [0,1)$ at which the reset is applied. Panel (a) shows Γ (black curve) with 50 isochrons evenly distributed in phase and the points labelled f_1, f_1^* (blue), and f_2, f_2^* (red) marked on Γ that lie, respectively, at (locally) minimal and maximal distances from the source $\boldsymbol{x}^*$. Panels (b) and (c) show the graphs of A_c as a function of ϑ_o and φ_d, respectively, with the branches labelled s_1, s_1^*, s_2, and s_2^* indicating the relation between ϑ_o and φ_d that achieves the singular phase reset.

$\gamma(\vartheta_o) \in \Gamma$ is shifted exactly to $\boldsymbol{x}^*$ by the vector $\boldsymbol{x}^* - \gamma(\vartheta_o)$; in other words, $\gamma(\vartheta_o)$ resets to $\boldsymbol{x}^*$ for the perturbation with amplitude $A_c = ||\boldsymbol{x}^* - \gamma(\vartheta_o)||$ in the unique direction $\boldsymbol{d} = (\boldsymbol{x}^* - \gamma(\vartheta_o))/||\boldsymbol{x}^* - \gamma(\vartheta_o)||$. In particular, the critical perturbation amplitude A_c achieves a local maximum or minimum when viewed as a function of ϑ_o or, alternatively, as a function of the angle φ_d of $\boldsymbol{d}$ as defined above.

The graph of A_c as a function of $\vartheta_o \in [0,1)$ is shown in Fig. 6(b), and similarly, the graph of A_c as a function of $\varphi_d \in [0,1)$ is shown in panel (c). The critical perturbation amplitude has a global minimum of $A_c \approx 0.2805$, at $\vartheta_o \approx 0.2981$ and at $\varphi_d \approx 0.6324$, given by the points labelled f_1 in panels (a), (b) and (c). Hence, any phase reset, in any direction, with perturbation amplitude $0 \leq A < 0.2805$, leads to a PTC that is a $1:1$ torus knot,

because the effect is a small shift of Γ that involves no interaction with $\boldsymbol{x}^*$. Similarly, A_c has a global maximum of $A_c \approx 1.3051$, labelled f_2 in Fig. 6, at $\vartheta_\mathrm{o} \approx 0.5971$ and at $\varphi_\mathrm{d} \approx 0.3701$. Any phase reset, in any direction, with perturbation amplitude $A > 1.3051$ leads to a PTC that is a $1:0$ torus knot, because the perturbed orbit no longer encloses $\boldsymbol{x}^*$. However, for any perturbation amplitude A in the range $[0.2805, 1.3051]$, there exists a direction angle $\varphi_\mathrm{d} \in [0, 1)$ such that PTC has a discontinuity; this direction angle is generically not unique.

The existing pairs $(\vartheta_\mathrm{o}, \varphi_\mathrm{d})$ that lead to a singular phase reset are given by the intersection points of the graphs in Fig. 6(b) and (c) with a horizontal line at the selected value of A_c; each such intersection point lies on one of four branches labelled s_1, s_2, s_1^* and s_2^*. How many there are depends on the level of A_c relative to the two other extremal points f_1^* and f_2^*: a local minimum and a local maximum of the distance from $\boldsymbol{x}^*$ of $A_c \approx 0.4134$ and $A_c \approx 0.8519$, respectively. For any phase reset with perturbation amplitude A in the range $(0.4134, 0.8519)$, the horizontal line with $A_c = A$ intersects all branches; hence, there are four particular phases along Γ that reset to $\boldsymbol{x}^*$, provided the associated specific direction angle $\varphi_\mathrm{d} \in [0, 1)$ is selected. However, when the perturbation amplitude is in the ranges $A \in (0.2805, 0.4134)$ or $A \in (0.8519, 1.3051)$ then there are only two such intersection points of $A_c = A$ with the two graphs, namely, on the branches s_1 and s_2, and on the branches s_2 and s_1^*, respectively.

4.1 Phase-resetting surface for fixed A

To illustrate the influence of the direction $\boldsymbol{d}$ of the perturbation, we now consider graph$(\mathcal{P}_A)$ in $(\vartheta_\mathrm{o}, \varphi_\mathrm{d}, \vartheta_\mathrm{n})$-space for different values of the perturbation amplitude A. As we discussed above, there are five different generic cases, corresponding to the five A-ranges generated by the values of A_c at the four extrema f_1, f_1^*, f_2 and f_2^*. They are presented in Figs. 7–9, where we show three copies or sheets of graph$(\mathcal{P}_A)$ over the extended ϑ_n-range $[-0.5, 2.5]$.

Figure 7 shows the phase-resetting surface graph$(\mathcal{P}_A)$ for $A = 0.2$ in panel (a), representing the A-interval $[0, 0.2805)$, and $A = 0.35$ in panel (b), representing $(0.2805, 0.4134)$. For $A = 0.2$ in panel (a), the PTC for any φ_d is a $1:1$ torus knot, which means that the three sheets of graph$(\mathcal{P}_A)$ are tilted so that the value of ϑ_n increases by 1 as ϑ_o varies from 0 to 1. For $A = 0.35$ in panel (b), however, this is no longer the case: the three sheets of graph$(\mathcal{P}_A)$ now all wrap around two singular vertical lines labelled s_1 and s_2; these singularities are at $(\vartheta_\mathrm{o}, \varphi_\mathrm{d}) \approx (0.2585, 0.2372)$ and $(\vartheta_\mathrm{o}, \varphi_\mathrm{d}) \approx (0.3346, 0.0258)$ in Figure 7(b), and they are created, for increasing A, when the global minimum f_1 at $A_c \approx 0.2805$ is passed in Fig. 6(b)

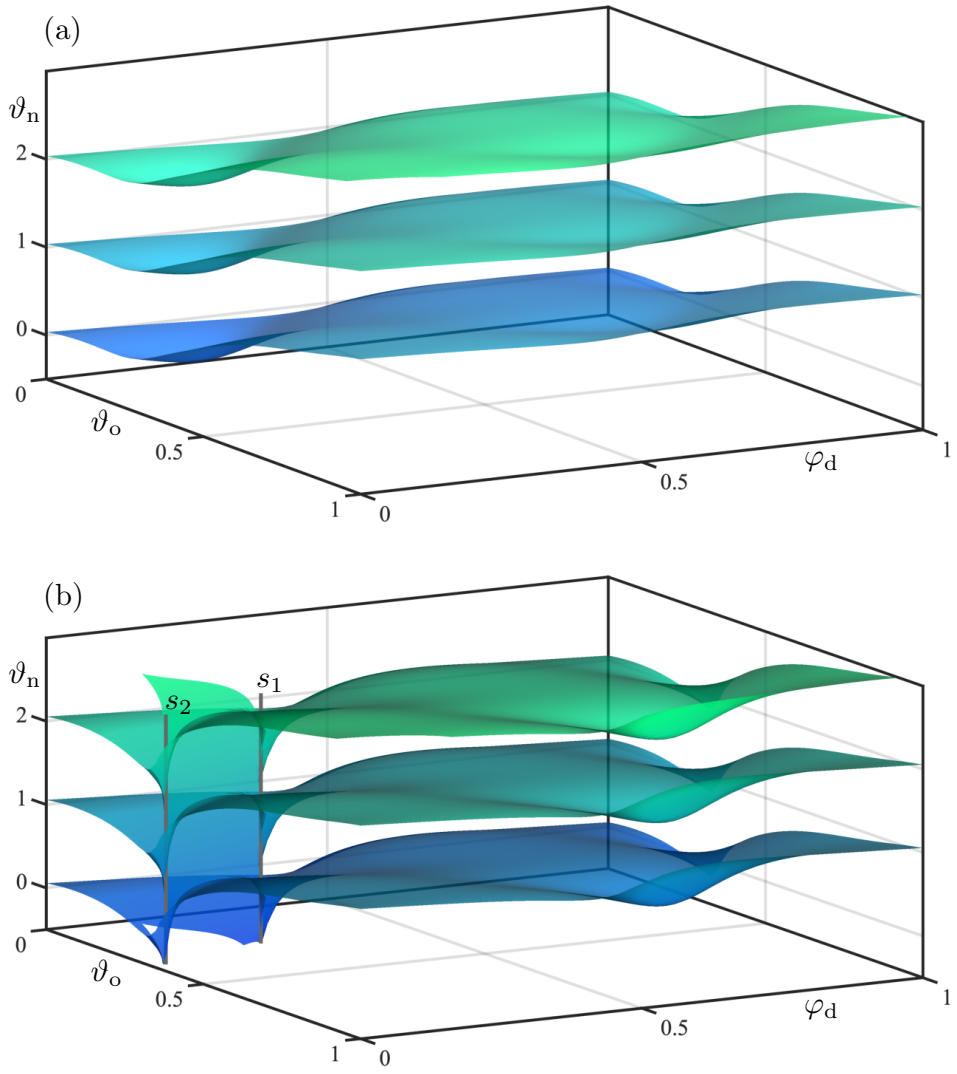

Figure 7: Three copies of the phase-resetting surface graph($\mathcal{P}_A$) of system (1) shown in $(\vartheta_o, \varphi_d, \vartheta_n)$-space for $\vartheta_n \in [-0.5, 2.5]$, with $A = 0.2$ in panel (a) and $A = 0.35$ in panel (b). The two vertical lines (grey) in panel (b) are at the singularities s_1 and s_2.

and (c) and the branches s_1 and s_2 are intersected. As a result, there is now the 'window' $(0.0258, 0.2372)$ of φ_d-values in between their 'singular' values corresponding to s_1 and s_2, for which the PTC is already a $1:0$ torus knot; for the complement $\varphi_d \in [0, 1) \setminus [0.0258, 0.2372]$, the PTC is still a $1:1$ torus knot. Exactly for the φ_d-values of the singularities s_1 and s_2, the PTC has

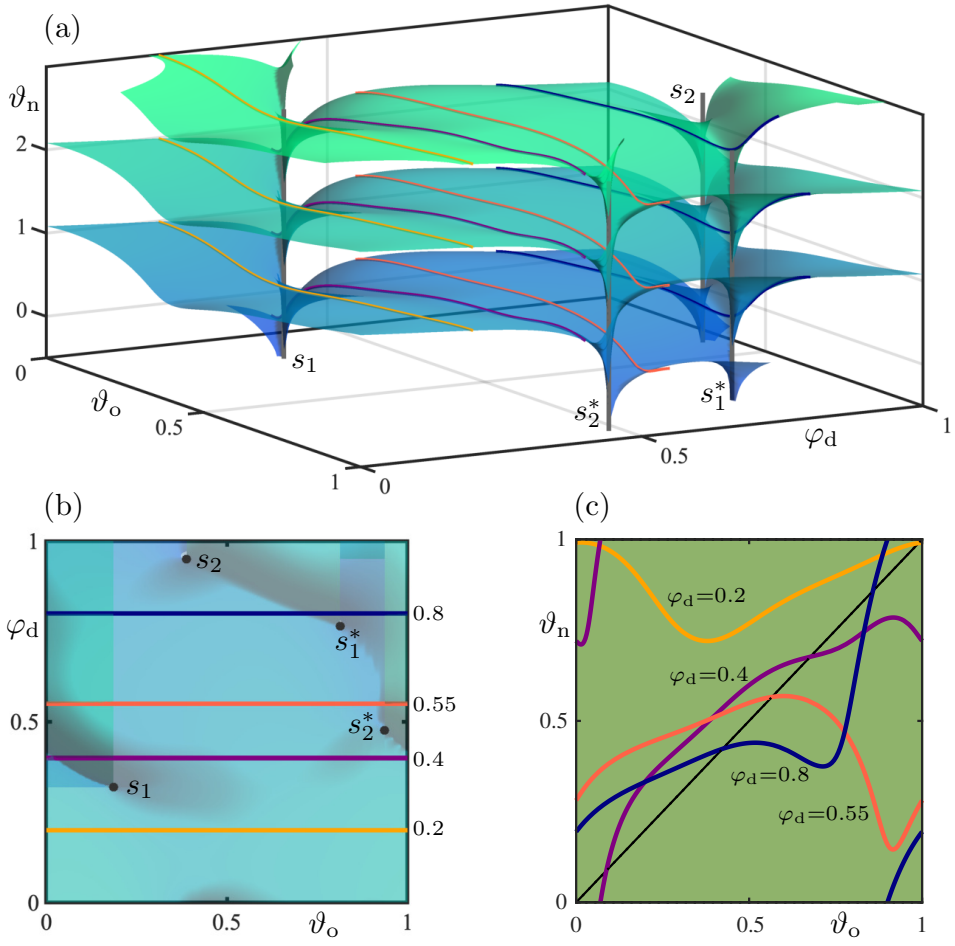

Figure 8: Panel (a) shows three copies of the phase-resetting surface graph($\mathcal{P}_A$) of system (1) in $(\vartheta_o, \varphi_d, \vartheta_n)$-space for $\vartheta_n \in [-0.5, 2.5]$ with $A = 0.6$, featuring four singularities s_1, s_2, s_1^*, and s_2^* (grey vertical lines); also shown are the four PTCs for $\varphi_d = 0.2$ (orange), $\varphi_d = 0.4$ (purple), $\varphi_d = 0.55$ (red), and $\varphi_d = 0.8$ (blue). Panel (b) is a projection of panel (a) onto the (ϑ_o, φ_d)-plane, and panel (c) shows the four PTCs on the fundamental square (green shading) of the $(\vartheta_o, \vartheta_n)$-plane.

a discontinuity as the one for $A = A_c$ shown in Fig. 1(b).

Figure 8 shows the phase-resetting surface graph($\mathcal{P}_A$) for $A = 0.6$, which is representative for the A-interval $(0.4134, 0.8519)$, where one finds the four singularities s_1, s_2, s_1^*, and s_2^*. Consequently, PTCs without discontinuities for this A-range are found in four φ_d-ranges. Panel (a) shows three sheets

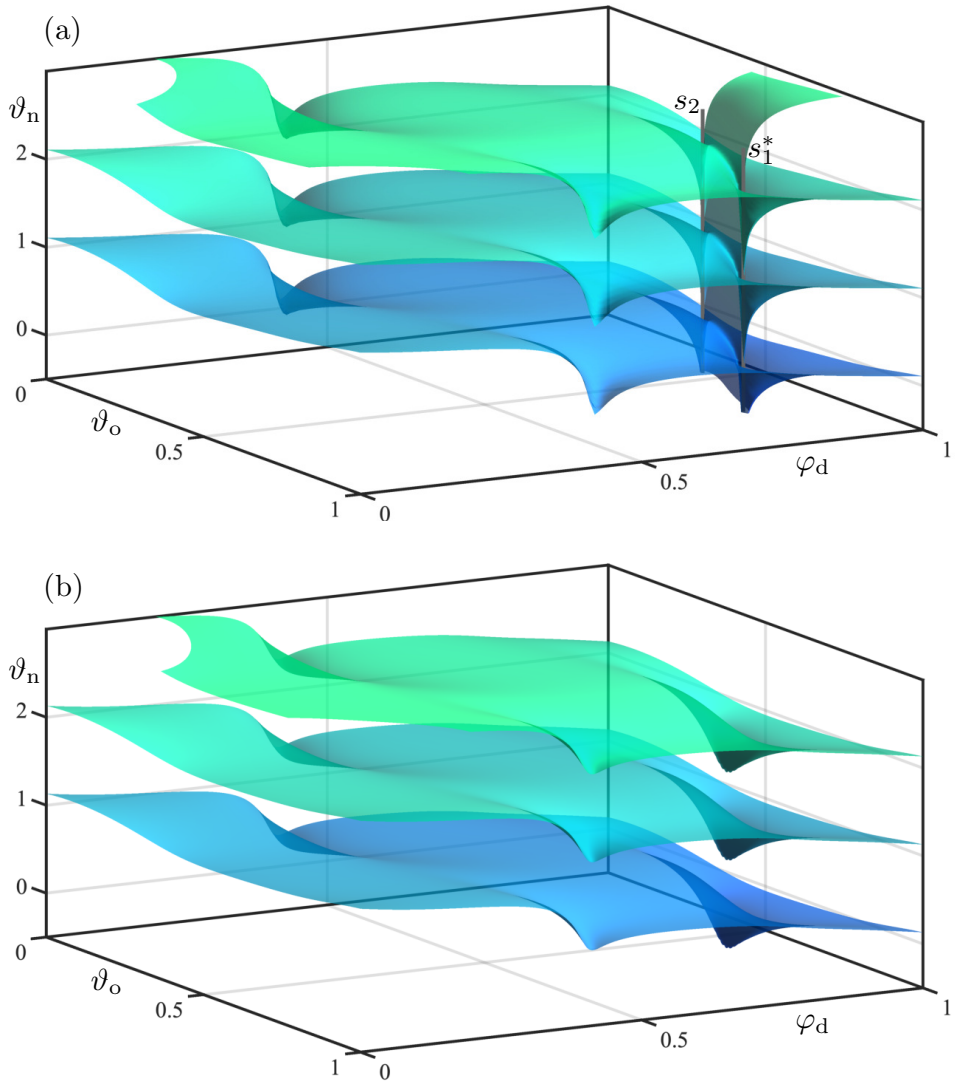

Figure 9: Three copies of the phase-resetting surface graph($\mathcal{P}_A$) of system (1) shown in $(\vartheta_o, \varphi_d, \vartheta_n)$-space for $\vartheta_n \in [-0.5, 2.5]$, with $A = 0.95$ in panel (a) and $A = 1.4$ in panel (b). The two vertical lines (grey) in panel (a) are at the singularities s_1^* and s_2.

of graph($\mathcal{P}_A$) in $(\vartheta_o, \varphi_d, \vartheta_n)$-space with the PTCs for the φ_d-values 0.2, 0.4, 0.55 and 0.8, and panel (b) provides a 'top-down' view in projection onto the (ϑ_o, φ_d)-plane; the four φ_d-ranges of PTCs are shown in panel (c) on the fundamental square. The singularities s_1 and s_2 are now at $(\vartheta_o, \varphi_d) \approx$

$(0.1857, 0.3188)$ and $(\vartheta_\mathrm{o}, \varphi_\mathrm{d}) \approx (0.3883, 0.9508)$, respectively. Moreover, there are two additional singularities s_1^* and s_2^* at $(\vartheta_\mathrm{o}, \varphi_\mathrm{d}) \approx (0.7651, 0.8135)$ and $(\vartheta_\mathrm{o}, \varphi_\mathrm{d}) \approx (0.9368, 0.4768)$, respectively. The phase-resetting surface graph$(\mathcal{P}_A)$ in Fig. 8(a) now wraps around all four singular vertical lines s_1, s_2, s_1^*, and s_2^*. Resets in directions corresponding to the associated singular φ_d-values lead to discontinuous PTCs. As panel (b) illustrates with a top view, there are now two 'windows' of φ_d-values for which the PTC is already a $1:0$ torus knot: the one between s_1 and s_2 for $\varphi_\mathrm{d} \in (0.9508 - 1, 0.3188)$, which is wider than in Fig. 7, and there is also a second 'window' between s_1^* and s_2^* for $\varphi_\mathrm{d} \in (0.4768, 0.8135)$. The PTCs for 0.2 and 0.55 in Fig. 8(c) are representative examples for these two φ_d-ranges of $1:0$ torus knots. In the two complementary φ_d-ranges, on the other hand, the PTC is still a $1:1$ torus knot, such as the PTCs for 0.4 and 0.8 in panel (c).

As A is increased, the singular points s_1 and s_2^* move closer together, and they merge and disappear at the local maximum f_2^* at $A_c \approx 0.4134$. Figure 9(a) shows the phase-resetting surface graph$(\mathcal{P}_A)$ for $A = 0.95$, which is representative for the A-interval $(0.8519, 1.3051)$. Again only two singularities remain, namely, s_1^* and s_2 at $(0.7445, 0.8236)$ and $(0.4559, 0.9126)$, respectively. The geometry of the phase-resetting surface graph$(\mathcal{P}_A)$ looks again as that in Fig. 7(b), but the difference is that the PTC is now a $1:0$ torus knot for almost all values of φ_d, except for the φ_d-range $(0.8236, 0.9126)$ in between s_1^* and s_2. As A is increased further through the global maximum f_2 at $A_c \approx 1.3051$, also s_1^* and s_2 disappear and graph$(\mathcal{P}_A)$ is as shown in Fig. 9(b) for the representative value $A = 1.4$. Here, the three sheets shown are such that there is no increase of ϑ_n when ϑ_o varies from 0 to 1 and, hence, all PTCs are $1:1$ torus knots. Notice, however, that the three sheets are just tilted differently: the value of ϑ_n increases by one as the direction angle φ_d varies from 0 to 1.

5 Conclusion and outlook

We studied phase resetting in the FitzHugh-Nagumo system (1), with a stable periodic orbit Γ surrounding a repelling focus $\boldsymbol{x}^*$, which is the only point not in the basin of attraction. Perturbations at phase ϑ_o, with amplitude A and in the direction $\boldsymbol{d}(\varphi_d)$, result in a new phase ϑ_n. We considered first the perturbations in the direction of increasing x, which is 'standard' for the FitzHugh-Nagumo system. The phase transition curve is the graph of the function $\mathcal{P}_A(\vartheta_\mathrm{o})$ that 'records' the phase ϑ_n after a perturbation at the point $\gamma(\vartheta_\mathrm{o}) \in \Gamma$ of strength A. The information of all PTCs can be represented by the phase-resetting surface, which is the graph of the function

$\mathcal{P}(\vartheta_\mathrm{o}, A) = \mathcal{P}_A(\vartheta_\mathrm{o})$ where A is also viewed as an input. This surface in $(\vartheta_\mathrm{o}, A, \vartheta_\mathrm{n})$-space effectively provides an atlas of phase resetting: each PTC is a 'slice' through graph($\mathcal{P}$) for the corresponding amplitude A. The phase-resetting surface has a singularity S when the perturbation moves a point on Γ exactly to the phaseless set $\boldsymbol{x}^*$. As Winfree already pointed out, moving the PTC across such a singularity changes it from being a $1:1$ to a $1:0$ torus knot, or vice versa, while at the critical amplitude A_c, the PTC is discontinuous. Owing to the spiralling nature of the isochrons near $\boldsymbol{x}^*$, the phase-resetting surface graph($\mathcal{P}$) wraps around a vertical line at the singular point S. This explains the existence of twin tangencies during the transition through such a 'spiralling' singularity, whereby the number of coverings of the fundamental ϑ_n-interval $[0, 1)$ by the PTC first increases and then decreases; we identified and illustrated several such twin tangencies of the FitzHugh-Nagumo system.

We also considered the influence of the direction angle φ_d on the PTC. To this end, we computed the phase-resetting surface graph($\mathcal{P}_A$) of the FitzHugh-Nagumo system (1) as a function of both ϑ_o and φ_d, which we showed for five representative values of the perturbation amplitude A. The transition with increasing A of the phase-resetting surface graph($\mathcal{P}_A$) in $(\vartheta_\mathrm{o}, \varphi_\mathrm{d}, \vartheta_\mathrm{n})$-space, which we illustrated in Figs. 7–9, is typical for the situation that a convex periodic orbit Γ of a planar vector field surrounds a single phaseless point $\boldsymbol{x}^*$ in the form of a repelling focus equilibrium. The aspects of what we mean by typical are: (1) the speed of rotation around Γ and locally around $\boldsymbol{x}^*$ are different, so that the isochrons spiral into $\boldsymbol{x}^*$; (2) there are two minima and two maxima of the distance $||\boldsymbol{x}^* - \gamma(\vartheta_\mathrm{o})||$ of $\boldsymbol{x}^*$ from any point on Γ; and (3) these are in general position (do not have the same values). The FitzHugh-Nagumo system (1) is also typical in that its isochrons and PTC are not known analytically and need to be found numerically. By solving suitably formulated multi-segment boundary value problems we computed a sufficient number of 'slices', from which the respective phase-resetting surfaces were then rendered; see [13, 14] for more details on the computational setup.

We remark that the example of the Van der Pol system discussed in [14] is not typical or generic: due to its invariance under rotation by π, the two minima and the maxima of the distance from the phaseless set are identical. Hence, one does not encounter the intermediate cases with just two singularities that we showed in Figs. 7(b) and Fig. 9(a). Moreover, we found that the rotation of the isochrons near $\boldsymbol{x}^*$, while nonzero, is not pronounced enough in the Van der Pol system to observe properly the wrapping of the phase-resetting surface around vertical lines of singularities. This can be considered a shortcoming of the Van der Pol example, which the FitzHugh-Nagumo system does not have. While we focused on how the PTC changes, we mention

that one can also consider the directional transition curve (DTC), obtained by considering ϑ_n as a function of φ_d for fixed ϑ_o and A. There is an interesting duality between the PTC and the DTC in terms of its properties near the singularity, which is discussed in considerable detail in [14].

The results we presented here for the FitzHugh-Nagumo system (1) are typical, but there are other generic scenarios one may encounter in planar vector fields. First of all, when the phaseless point $\boldsymbol{x}^*$ is very close to a convex periodic orbit Γ surrounding it, the distance $||\boldsymbol{x}^* - \gamma(\vartheta_\mathrm{o})||$ may only have a single minimum and a single maximum. Moreover, Γ might not be convex, which could lead to the existence of more than two pairs of (local) minima and maxima of the distance, which are again, generically, in general position. The transition for increasing A of the phase-resetting surface graph($\mathcal{P}_A$) in $(\vartheta_\mathrm{o}, \varphi_\mathrm{d}, \vartheta_\mathrm{n})$-space through such different sequences of minima and maxima follows immediately from the arguments we presented here. A more interesting situation is that the phaseless set inside Γ no longer consists of a single point. For example, it could be a disk bounded by a repelling periodic orbit, or be the closure of the stable manifold of a saddle equilibrium; see [8, 9] for such examples. In either case, the PTC will be discontinuous at more than just a single point. The associated consequences for the phase-resetting surface can be investigated in the geometric spirit we adopted here, but this remains an interesting subject for future research. Finally, a challenging subject of our ongoing research concerns phase resetting in higher-dimensional systems. The issue here is that the basin boundary of the attracting periodic orbit under consideration may be very complicated; in particular, it will contain the (generally higher-dimensional) stable manifolds of any saddle equilibria and periodic orbits.

References

[1] E. N. Best. Null space in the Hodgkin-Huxley equations. A critical test, *Biophysics Journal*, **27**(1): 87–104, 1979. (doi: `10.1016/S0006-3495(79)85204-2`)

[2] H. Dankowicz and F. Schilder. *Recipes for Continuation* (SIAM Publishing, 2013). (doi: `10.1137/1.9781611972573`)

[3] G. B. Ermentrout and D. H. Terman. *Mathematical Foundations of Neuroscience*. Interdisciplinary Applied Mathematics, Vol. 35 (Springer-Verlag, 2010). (doi: `10.1007/978-0-387-87708-2`)

[4] G. B. Ermentrout, L. Glass and B. E. Oldeman. The shape of phase-resetting curves in oscillators with a saddle node on an invariant circle bifurcation. *Neural Computations*, **24**(12): 3111–3125, 2012. (doi: 10.1162/NECO_a_00370)

[5] R. FitzHugh. Impulses and physiological states in theoretical models of nerve membrane. *Biophysical Journal* **1**(6): 445–466, 1961. (doi: 10.1016/S0006-3495(61)86902-6)

[6] L. Glass and A. T. Winfree. Discontinuities in phase-resetting experiments, *American Journal of Physiology*, **246**(2): R251–R258, 1984. (doi: 10.1152/ajpregu.1984.246.2.R251)

[7] J. Guckenheimer. Isochrons and phaseless sets, *Journal of Mathematical Biology*, **1**(3): 259–273, 1975. (doi: 10.1007/BF01273747)

[8] J. Hannam, B. Krauskopf and H. M. Osinga, Global isochrons of a planar system near a phaseless set with saddle equilibria, *The European Physical Journal – Special Topics*, **225**(13) (2016) 2645–2654. (doi: 10.1140/epjst/e2016-60072-4)

[9] J. Hannam, B. Krauskopf and H. M. Osinga, Isochron foliations and global bifurcations: a case study, *Transaction of Mathematics and its Applications*, **6**(2) (2022) tnac002. (doi: 10.1093/imatrm/tnac002)

[10] M. W. Hirsch, C. C. Pugh, and M. Shub. *Invariant Manifolds*. Lecture Notes in Mathematics, Vol. 583 (Springer-Verlag, 1977). (doi: 10.1007/BFb0092042)

[11] P. Langfield, B. Krauskopf and H. M. Osinga. Solving Winfree's puzzle: the isochrons in the FitzHugh–Nagumo model, *Chaos*, **24**(1): 013131, 2014. (doi: 10.1063/1.4867877)

[12] P. Langfield, B. Krauskopf and H. M. Osinga. Forward-time and backward-time isochrons and their interactions, *SIAM Journal on Applied Dynamical Systems*, **14**(3): 1418–1453, 2015. (doi: 10.1137/15M1010191)

[13] P. Langfield, B. Krauskopf and H. M. Osinga. A continuation approach to computing phase resetting curves, in O. Junge, O. Schütze, G. Froyland S. Ober-Blöbaum and K. Padberg-Gehle (eds.) *Advances in Dynamics, Optimization and Computation. SON 2020*, Studies in Systems, Decision and Control, Vol. 304 (Springer-Verlag, 2020), pp. 3–30. (doi: 10.1007/978-3-030-51264-4_1)

[14] K. H. Lee, N. G. R. Broderick, B. Krauskopf and H. M. Osinga. Phase response to arbitrary perturbations: Geometric insights and resetting surfaces, *Discrete & Continuous Dynamical Systems — Series B* Early Access (2024). (doi: 10.3934/dcdsb.2024140)

[15] J. Nagumo, S. Arimoto and S. Yoshizawa. An active pulse transmission line simulating nerve axon. *Proceedings of the IRE* **50**(10): 2061–2070, 1962. (doi: 10.1109/JRPROC.1962.288235)

[16] H. M. Osinga and J. Moehlis. Continuation-based computation of global isochrons, *SIAM Journal on Applied Dynamical Systems*, **9**(4): 1201–1228, 2010. (doi: 10.1137/090777244)

[17] A. Pérez-Cervera, T. M. Seara and G. Huguet. A geometric approach to phase response curves and its numerical computation through the parameterization method, *Journal of Nonlinear Science*, **29**(6): 2877–2910, 2019. (doi: 10.1007/s00332-019-09561-4)

[18] N. W. Schultheiss, A. A. Prinz and R. J. Butera. *Phase Response Curves in Neuroscience: Theory, Experiment, and Analysis*. Computational Neuroscience, Vol. 6 (Springer, 2012). (doi: 10.1007/978-1-4614-0739-3)

[19] A. T. Winfree. Time and timelessness in biological clocks, in J Urquhart and F. E. Yates (eds.) *Temporal Aspects of Therapeutics*. ALZA Conference Series, Vol. 2 (Springer-Verlag, 1973), pp. 35–49. (doi: 10.1007/978-1-4684-2847-6_4)

[20] A. T. Winfree. Patterns of phase compromise in biological cycles, *Journal of Mathematical Biology*, **1**(1): 73–93, 1974. (doi: 10.1007/BF02339491)

[21] A. T. Winfree. *The Geometry of Biological Time*, 2nd ed. Interdisciplinary Applied Mathematics (IAM), Vol. 12 (Springer-Verlag, 2001). (doi: 10.1007/978-1-4757-3484-3)

[22] A. T. Winfree. Sudden cardiac death: A problem in topology, *Scientific American* **248**(5): 144–161, 1983. (doi: 10.1038/scientificamerican0583-144)